Progress in Organic Coatings 183 (2023) 107754

Contents lists available at ScienceDirect

Progress in Organic Coatings

journal homepage: www.elsevier.com/locate/porgcoat

Smart controlling on the bi-stable state of bio-inspired multifunctional coatings for anti-/de-icing applications

Xinlin Li [a], Zhe Zhao [a], Yan Liu [b,*], Yanju Liu [c,*], Jinsong Leng [a,*]

[a] Centre for Composite Materials and Structures, Harbin Institute of Technology (HIT), Harbin 150080, PR China
[b] Key Laboratory of Bionic Engineering (Ministry of Education), Jilin University, Changchun 130022, PR China
[c] Department of Astronautical Science and Mechanics, Harbin Institute of Technology (HIT), Harbin 150080, PR China

ARTICLE INFO

Keywords:
Multifunctional coatings
Hierarchical interface
Reversible wettability
Bi-stable state
Anti-/de-icing

ABSTRACT

Outdoor equipment can suffer from functional failure in winter due to ice accumulation. Although functional materials are widely recognized as promising candidates for anti-icing and de-icing applications, ice inevitably accretes on surfaces at extremely low temperatures and high humidity. If surfaces display reversible superhydrophobic and slippery performance, similar to Lotus leaves and fish skin, it will significantly improve the anti-icing and de-icing performance. This study proposes a novel type of multifunctional coating that could smartly reverse between superhydrophobic and slippery properties on demand. The superhydrophobic coatings with diverse morphologies were obtained by employing different sizes and shapes of nanoparticles. Due to the low adhesion and photothermal properties, the superhydrophobic samples presented good freezing rain prevention and snow-melting performances by outdoor tests in winter. The samples with slippery surfaces were produced by infusing dodecane on the as-prepared superhydrophobic surface. Both the superhydrophobic and slippery surfaces can effectively propel the water droplets, prolong the freezing time and enhance ice removal performance in an extremely cold environment. Therefore, the coated samples with bi-stable states (i.e., superhydrophobic and slippery states) were successfully achieved with the potential to be widely applied under different service environments. This facile strategy will provide the possibility for developing novel materials with smart reversible wettability for anti-icing and de-icing applications.

1. Introduction

With ice accumulation in winter, the functions of aircraft or outdoor equipment may severely degrade and even result in high operational risks [1,2]. However, the traditional ice prevention methods have the shortcomings of high energy consumption and potential environmental pollution with complex operational challenges at large scale. Hence, developing active anti-/de-icing strategies becomes urgently needed [3,4]. The anti-icing strategy prevents water/ice accumulation before adhesion occurs, while the de-icing strategy removes ice actively with/without external stimuli.

Nature has provided numerous examples of materials with unique structures that can be potentially applied to prevent ice accumulation [5–7], such as lotus leaves and fish. Inspired by the natural wetting phenomenon, functional materials can potentially achieve active anti-icing and de-icing strategies. For example, superhydrophobic materials are designed by mimicking the self-cleaning functions of a lotus leaf. Various superhydrophobic surfaces with improved functions have been developed by combining physical and chemical methods, such as laser ablation [8], machining [9], 3D printing [10,11], chemical etching [12], etc. The spraying method is commonly used in surface coating [13,14], easily scalable, low-cost, and easy to process. For example, Celik et al. [15] developed the superhydrophobic coatings of two-tier hierarchical structures under optimized spraying conditions. Due to the complex shapes and sizes of various facility structures, spray coating is the most facile technique for depositing superhydrophobic layers at an industrial scale for anti/de-icing applications. However, such superhydrophobic coatings can suffer from chemical degradation and mechanical wear with poor icephobic performance under extreme conditions. Water droplets inevitably bond on superhydrophobic surfaces in a high-humidity environment, leading to the degradation of interfacial functions [16]. Especially, the tiny droplets may occupied the air pockets and anchor at the hierarchical structures at low-temperature [17]. Thus, anti-icing can fail on a simple superhydrophobic surface, and some novel

* Corresponding authors.
E-mail addresses: yj_liu@hit.edu.cn (Y. Liu), lyyw@jlu.edu.cn (Y. Liu), lengjs@hit.edu.cn (J. Leng).

https://doi.org/10.1016/j.porgcoat.2023.107754
Received 4 April 2023; Received in revised form 9 June 2023; Accepted 11 June 2023
Available online 17 June 2023

hybrid, multifunctional composite materials need to be developed to improve the anti-icing and de-icing performance under extreme conditions. In contrast to the mechanical and chemical methods, electro-/photo-thermal methods are more efficient with precise control in removing ice. Wang et al. [18] developed a photothermal superhydrophobic polyimide surface by laser-induced graphene (LIG) deposition technology. It offers high light absorbance with ultra-long freezing delay time under sunlight irradiation. In addition, Zhao et al. [19] proposed a multifunctional anti-icing and de-icing strategy by combining electrothermal and photothermal effects on a superhydrophobic surface. Consequently, developing multifunctional superhydrophobic materials for efficient anti-i/de-icing applications is becoming a new trend.

Inspired from fish skin, a slippery surface is another popular type of icephobic coatings [20–23]. Long et al. [24] first fabricated a superhydrophobic surface with micro/nanoscale rough structures and the slippery surface was developed by infusing silicone oil. Results showed that the slippery surface offered better anti-icing performance than the non-slippery superhydrophobic surface. Carlotti et al. [25] reported a simple method of fabricating a slippery surface by adding silicon oil onto a candle-soot-covered stretchable double-sided tape. The ice removal strength was reduced to as low as 20 kPa. Moreover, some studies discussed the possibility of introducing phase-change materials as the lubricant for smart icephobic applications due to their stimuli-response to environmental changes [26,27]. The phase change enables them to store and release heat when the temperature changes. Chatterjee [28] presented the icephobic property of a superhydrophobic surface and phase-change slippery surface by selecting the phase-switching liquids. The presence of phase-changing materials prolonged the freezing delay time and reduced frost condensation by altering the condensation process [29]. Wang et al. [30] developed a phase-change slippery material by introducing peanut oil as the lubricant into the porous PDMS matrix, which enhanced the anti−/de-icing stabilities. However, the lubricants on slippery surface may suffer from degradation, leakage, and vaporization, resulting in the short life span in real applications. And the degraded slippery surface may greatly reduce its icephobic performance. Fewer reports focus on the renewable behavior and long-term performance of a slippery surface for icephobic applications.

Combining the advantages of lotus leaf and fish skin, in this work, we developed a multifunctional coating that could smartly reverse between superhydrophobic surfaces and slippery surfaces on demand. The superhydrophobic coating EP-4 can reach a high water contact angle (WCA) of ~151 ± 1° and a low sliding angle (WSA) of 18 ± 3°. Its micro-nano hierarchical structures provided sufficient air pockets for superhydrophobic performance and also an enhanced storage capacity of lubricants. The reversible wettability property of these featured coatings was investigated, and the stability was demonstrated by repeated cycles. At the superhydrophobic state, the as-prepared coatings presented good anti-icing performance by preventing the adhesion of freezing water and an effective de-icing performance due to the photothermal property. Furthermore, the as-prepared superhydrophobic coatings infused with dodecane displayed the slippery and ultra-low friction property, where the WCA and WSA were ~ 112° and ~ 6°, respectively. At this state, the as-prepared coating presented enhanced water sliding, freezing delay, and ice reduction performance. Therefore, this paper provides a novel strategy to prepare multifunctional coatings with wettability-reversible performance for anti-icing and de-icing improvement.

2. Experimental section

2.1. Materials

Commercially available aluminum alloy, glass, and tinplate were selected as the substrates for different applications. Epoxy resin (E51) and curing agent were provided by Kunshan Jiulimei electronic materials Co., Ltd. (China). Multi-walled carbon nanotubes (MWNTs) were purchased from Suzhou Tanfeng Graphene Technology Corporation. Silica (SiO_2) nanoparticles, hexadecyltrimethoxysilane (HDTMS), ferroferric oxide (Fe_3O_4), and benzyl alcohol provided by Aladdin reagent (Shanghai, China).

2.2. Preparation process of multi-functional coatings

First, MWNTs, Fe_3O_4, and SiO_2 were dispersed in 100 mL of ethyl acetate at the weight ratio of 3:7:5 by mechanically stirring for 10 min. Subsequently, 0.5 mL hexadecyltrimethoxysilane was added to the above solution and mechanically stirred for 6 h at room temperature. Then, epoxy resin (E51) was fully dissolved in the solution at the total weight ratio of x:1.5, where 1.5 is the weight of added particles, together with 5 mL benzyl alcohol. In this work, x was 3, 3.5, 4, 4.5, and 5 g. The corresponding samples were labeled EP-3, EP-3.5, EP-4, EP-4.5, and EP-5. After mechanically stirring for 6 h, the curing agents of E51 were added at a ratio of 4:1, followed by mechanical stirring for 1 h. Afterward, the uniform solution was sprayed onto the aluminum alloy, glass, and tinplate to form a thin film coating. The spraying was conducted at 0.6 MPa air pressure at a spraying distance of 20 cm with a spraying time of 5 s. The superhydrophobic coatings were transferred to the oven and cured at 100 °C for 2 h. And the slippery coatings were prepared by depositing a certain amount of dodecane on the selected superhydrophobic coatings. The excessive dodecane was removed by lifting the coated sample. Consequently, the superhydrophobic and slippery coatings can be prepared by repeatedly dropping the dodecane and washing it with ethanol.

2.3. Characterization of as-prepared multi-functional coatings

2.3.1. Surface characterizations

A scanning electron microscope (SEM, TESCAN AMBER, Czech) and a 3D optical microscope (Bruker Contour GT-X, Germany) were employed to investigate the surface morphologies and roughness, respectively. The chemical characters were analyzed by Energy Dispersive Spectroscopy (EDS, Oxford Ultimately MAX40, UK) and Fourier Transform Infrared Spectroscopy (FTIR, Thermo Nicolet iS5, USA). The surface wettability of superhydrophobic coatings and slippery coatings was measured by a contact angle meter (Shengding-100S, China) at room temperature, and the volume of the tested water droplets was 5 μL. Two high-speed cameras (Phantom Miro C320 and Phantom V711, USA) captured the water dynamics on the as-prepared coatings from the top and side directions.

2.3.2. Investigation of anti-/de-icing performance on the superhydrophobic coatings

The outdoor experiments were carried out in winter at Harbin, China. The environmental temperature was −14 °C, and the bare surface and superhydrophobic coated samples were installed on a wood plate with a fixed tilted angle of 30° relative to the horizontal plane. To investigate the prevention of freezing rain, water and the tested samples were placed in outdoors for over 10 min before the test. A sprayer was utilized to generate the micro-size water droplets (average diameters ~100 μm), fixed at a distance of 20 cm from the sample. The coalescence process was captured by a camera. For de-icing performance test, the samples were placed for a night at the temperature of −10 °C to cover them with snow. The de-icing was carried out by illuminating IR light (808 nm, 1 W) or exposing them to sunlight.

2.3.3. Investigation of anti-/de-icing performance on the improved slippery coatings

The in-house anti−/de-icing performances were investigated by a homemade apparatus illustrated in Fig. S1. In the anti-icing test, the freezing delay performance was evaluated by recorded the icing process and temperatures of water droplets (50 μL) on the tested samples in a sealed environment simultaneously. The freezing delay time began to be

recorded when the temperature of the hermetic space was decreased to 0 °C. For the de-icing test, the ice shear strength (ISS) was evaluated by a high-precision force sensor when the ice columns were removed from different tested samples.

3. Results and discussion

3.1. Surface morphologies and chemicals

Fig. 1 illustrates the spray coating method for preparing the superhydrophobic and slippery coatings. The epoxy resin ratio is important in achieving different surface morphology and properties. As shown in Fig. 2a, the EP-3 sample shows some surface crackles, ranging from 5 to 20 μm, and numerous branches. Fig. 2a_1 shows several small gaps within the micro-structures. Similar surface features were observed on EP-3.5. Although its crackles were wider than that on the EP-3, fewer branches were observed. No defects were found on the micro protrudes from the highly magnified images in Fig. 2a_2 and b_2. Therefore, it could be concluded that E51 acted as an effective binder in the preparation of superhydrophobic coatings, and the low ratio of EP could result in defects and reduced functionality. With increasing the E51 content, the as-prepared coatings increased the roughness uniformly. As shown in Fig. 2c and c_1, the surface of EP-4 displayed the hierarchical structures composed of numerous papillae at the micro/nano scales. The highly magnified SEM image in Fig. 2c_2 reveals that the papillae were covered by plenty of nano protrudes and wrinkles, which can improve air storage capacity dramatically [31]. In contrast to EP-4, as shown in Fig. 2d and d_1, the rougher morphology was observed on the coatings of EP-4.5, and the diameters of micro protrude increased (about ~20 μm). Meanwhile, the highly magnified SEM image of EP-4.5 shows more wrinkles and nano protrudes with an increased aspect ratio. Some larger agglomerates were formed on the as-prepared coatings of EP-5, where the diameters of micro protrude were beyond ~30 μm, as shown in Fig. 2e and e_1. The high-magnification SEM image in Fig. 2e_2 shows fewer nanoprotrudes and wrinkles due to the higher E51 content.

Besides, a 3D optical microscope was employed to investigate the roughness of as-prepared coatings, crucial to the superhydrophobic property. As shown in Fig. 2a_3 to e_3, the as-prepared coatings became rougher as the EP content increased, consistent with the SEM images. The roughness was evaluated by the average roughness (Ra) and the root means square roughness (Rq) values. As listed in Table S1, the Ra and Rq show an increasing trend upon increasing the EP content. Especially, the EP-4 and EP-4.5 exhibited relatively high Ra and Rq values of 8.529 and 11.721 μm, and 8.991 and 11.776 μm, respectively. However, the Ra and Rq values of the EP-5 were decreased relative to EP-4.5 due to the high EP content. Therefore, higher concentrations of EP result in rougher structures, while the excessive content of EP negatively influence surface morphology and roughness.

The unique structures of as-prepared coatings were formed by the aggregations of nanoparticles with different sizes and shapes, as shown in Fig. 3. From the TEM images, it shows that the long fibrous CNTs with a diameter of ~10 nm has acted as the supporting structures attached by the Fe_3O_4 and SiO_2 spherical particles. Moreover, the size of the Fe_3O_4 particles is ten times larger than the SiO_2 particles. The deposition of the Fe_3O_4 and SiO_2 particles between the CNTs fibers improves the complexity and roughness of the as-prepared hierarchical structures [33]. To investigate the distribution of chemical compositions, the elemental mapping of the as-prepared EP-4 was measured by EDS. From Fig. 3d, the EDS spectrum shows that the EP-4 surface is formed with C, O, Si, and Fe, and the corresponding weight contents of 67.82 %, 24.14 %, 3.54 %, and 4.5 %, respectively. Meanwhile, all elements, especially Si and Fe, were evenly distributed on the coating surface, indicating uniform surface composition, as shown in Fig. 3e. Furthermore, characteristic vibrational peaks of the as-prepared EP-4 coating were evaluated by FTIR spectrum in Fig. S2. The peak at 3441 cm^{-1} is assigned to the stretching of the O—H. The peaks at 2924 and 1457 cm^{-1} are attributed to the asymmetrical C—H stretching and bending of the alkyl groups [34]. Additionally, the peaks at 1103 and 1036 cm^{-1} are ascribed to the Si-O-Si group [35], and the peak at 566 cm^{-1} is assigned to the vibration of Fe—O group [36]. The FTIR results demonstrated that the as-prepared surface was covered by micro/nanoparticles modified by hexadecyltrimethoxysilane, forming the low surface energy state.

3.2. Reversible wettability and self-cleaning property

To evaluate the wettability of the coatings with different EP contents, the water contact angle (θ_{CA}) and water sliding angle (θ_{SA}) were measured. As shown in Fig. 4a, the θ_{CA} decreased when the EP content increased, in contrast to the trend of surface roughness. The EP-3 presented the highest θ_{CA} of 155 ± 2° with the corresponding θ_{SA} of 18 ± 3°. It should be noticed that the θ_{CA} of EP-4 decreased to 151 ± 1° while the θ_{SA} has no obvious change. However, the θ_{CA} of EP-4.5 and EP-5 were much lower than 150°, while the θ_{SA} was over 90°, exhibiting superhydrophobic and high adhesion performance. The superhydrophobic property of a coated surface is dominated by both surface morphology and chemical compositions [37]. The addition of EP led to the surface coating of each particle, leading to the degradation of the superhydrophobic performance. Here, the as-prepared sample of EP-4 was selected as the best coating for further investigation.

Besides, superhydrophobic surfaces can be developed to transfer confidential information. To achieve information transfer, as shown in Fig. 4b, the superhydrophobic substrates were covered by a copper protective mask with target characters and irradiated by oxygen atmosphere plasma for 30 s. When the patterned surface was wetted by water, as displayed in Fig. 4c, the characters of "HIT" were completely wetted instead of superhydrophobic regions. It proved that the information on the protective mask had been successfully transferred onto the superhydrophobic surfaces. Therefore, the complex shapes or patterns can be

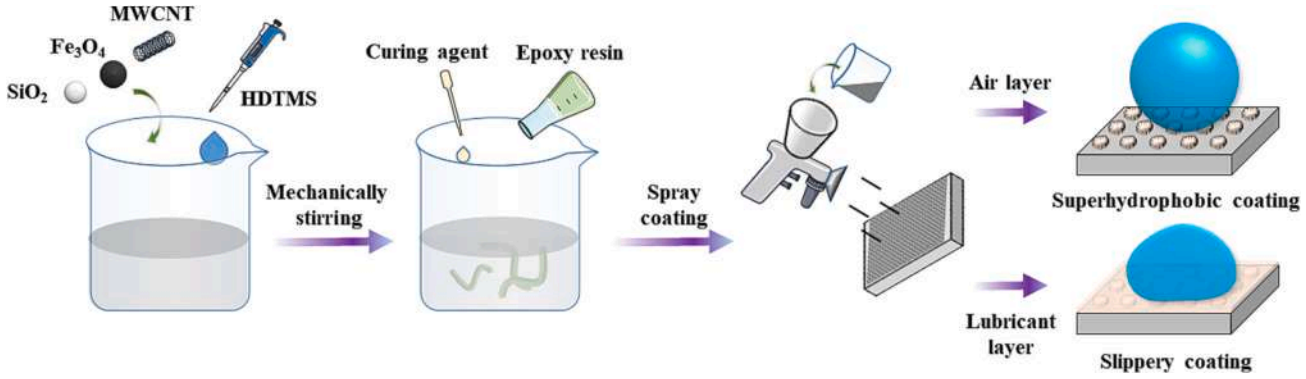

Fig. 1. Schematic of the preparation process of as-prepared multifunctional coatings.

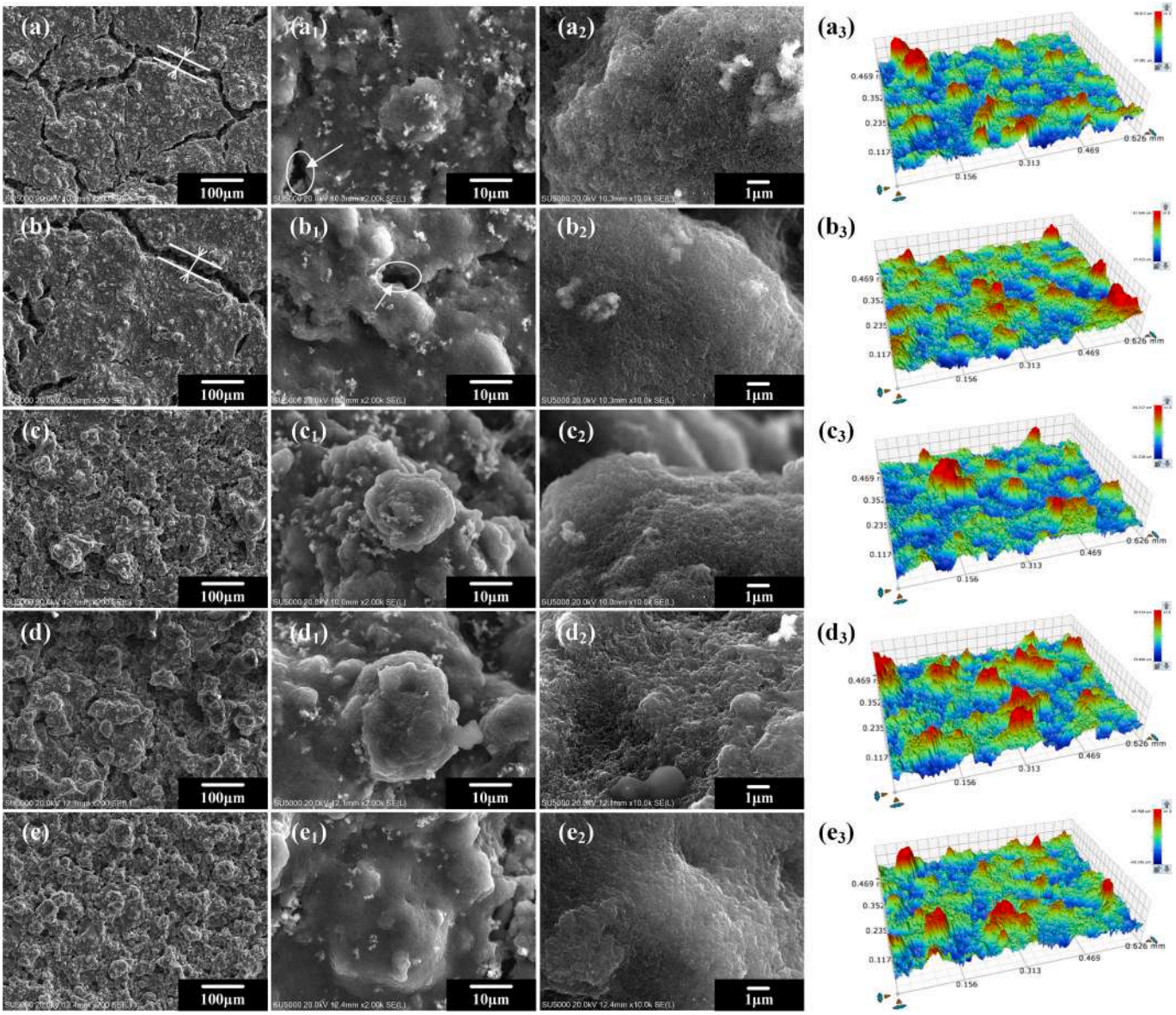

Fig. 2. SEM images from surface of (a, a_1, a_2) EP-3, (b, b_1, b_2) EP-3.5, (c, c_1, c_2) EP-4, (d, d_1, d_2) EP-4.5, and (e, e_1, e_2) EP-5 at the magnifications of 200×, 2000× and 10,000×, and a_3, b_3, c_3, d_3, and e_3 are the corresponding 3D optical microscope images, respectively.

potentially transferred onto the superhydrophobic surfaces for future applications.

The challenge to the coatings in outdoor applications is that it inevitably suffers from the contamination of dust or particles. To investigate the self-cleaning behavior of the superhydrophobic coatings, silicon particles were deliberately sprinkled on the EP-4 coating, as shown in Fig. 4d. It is observed that the silicon particles were easily removed by water droplets at the tilt angle of 12°, indicating its good self-cleaning property like the lotus leaves. Meanwhile, the silicon particles could be removed by water droplets if the coating was immersed in dodecane (dyed orange), as shown in Fig. 4e. At this time, the air pockets on the coatings were replaced by dodecane, presenting a good slippery property. Interestingly, the wettability of the coatings can reverse from superhydrophobicity to slippery and vice versa. As shown in Fig. 4f, the coatings presented good superhydrophobicity before the infusion of dodecane with the θ_{CA} of ~150° and θ_{SA} of ~23°. After being infused with dodecane, the coatings presented good slippery properties with θ_{CA} and θ_{SA} of ~112° and ~ 6°, respectively. Noticeably, the slippery surface could be reversed to the superhydrophobic surface when washed with ethanol and dried by hair drier, as shown in the insets of Fig. 4f, with a recovered θ_{CA} of ~150° and the θ_{SA} of ~28°. Even after 9 cycles of infusing and washing, the coatings showed reversible wettability performance. Consequently, the superhydrophobic coatings can efficiently inhibit the ice nucleation at the initial cooling stage and effectively remove the adhered ice when the coatings are transferred to be slippery. Therefore, the icephobic capacity of the coated surface is improved by smartly controlling the surface wettability.

3.3. *Anti-/de-icing performance on the as-prepared superhydrophobic coatings*

The superhydrophobic coatings EP-4 are expected to offer good anti−/de-icing performance for outdoor applications. Freezing rain is the most dangerous weather that may result in the functional degradation of facilities. To investigate the prevention ability against freezing rain, the superhydrophobic coatings EP-4 were placed on a wood plate with a bare tin plate for comparison. The outdoor temperature was −14 °C, and the tilted angle was 30°. The water was kept outdoors for

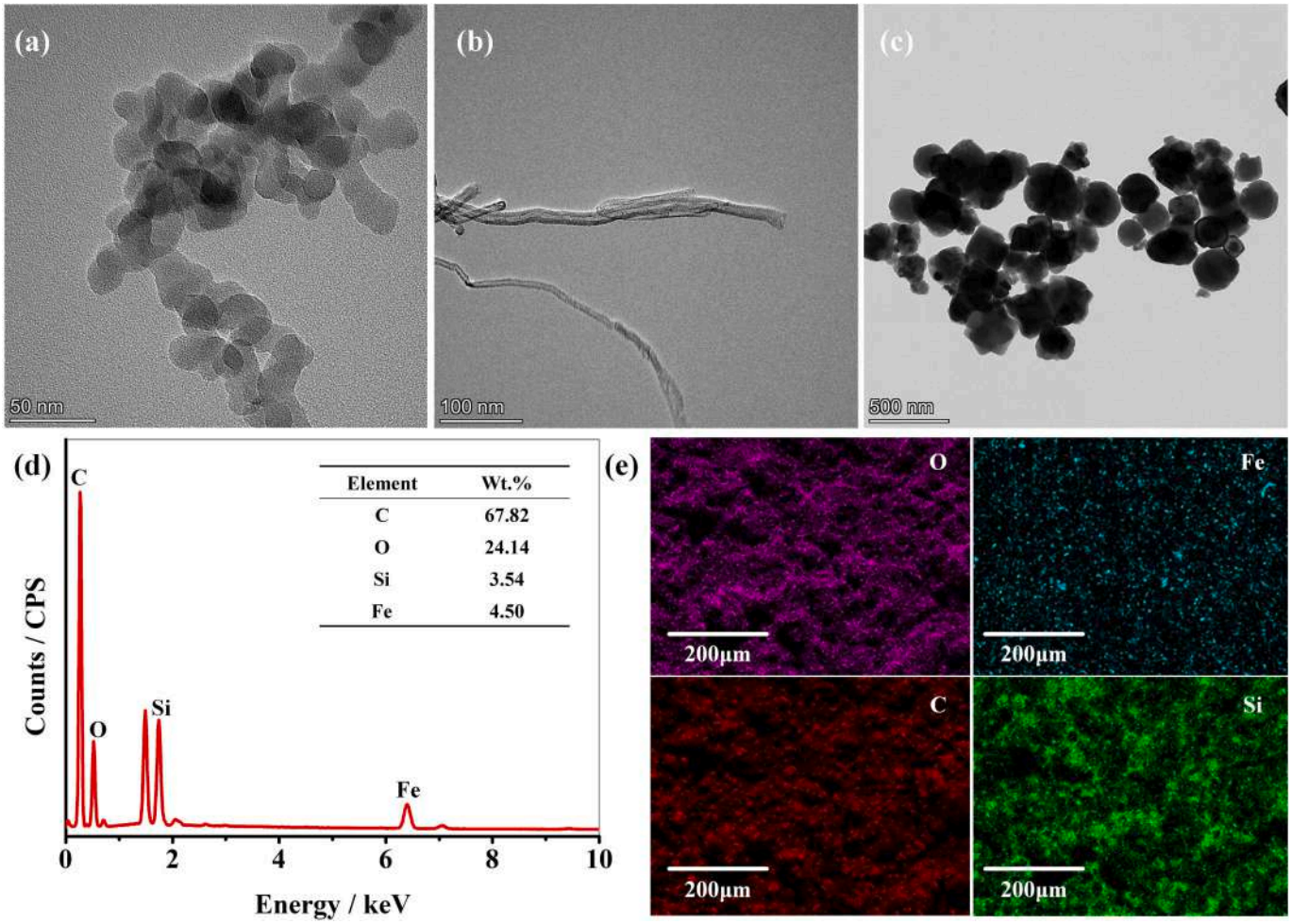

Fig. 3. TEM images of the nano-particle (a)CNTs, (b)Fe_3O_4, (c)SiO_2. (d) EDS spectra of as-prepared EP-4, and (e) EDS mapping images of characteristic chemicals.

about 10 min to form supercold droplets before being sprayed onto the samples by a handheld sprayer at a distance of 20 cm. The average diameters of the spraying water droplets were around 100 μm.

From the optical pictures in Fig. 5a and Supporting Video S1, water droplets gradually accumulated on the coated and bare surfaces after being sprayed 11 times. However, it was observed that the bare surface was quickly wetted, while the superhydrophobic surface was only covered by a tiny amount of water droplets. After spraying 21 times, the bare surface was fully covered by water/ice, as shown in Fig. 5a_1. But parts of the regions on the superhydrophobic surface were still free from water droplets. The average diameters of frozen water droplets were smaller than ~3 mm. After being sprayed 49 times, the average diameters of the frozen water droplets increased to ≈5 mm, see Fig. 5a_2. Besides, the adjacent regions of the water droplets on coatings were refreshed by coalescences if the average diameters of water droplets could reach ≈1 cm, see Fig. 5a_3. Following the proceeding of the condensation, the size of water droplets increases, as shown in Fig. 5b. It had a high ice removal efficiency due to the low adhesion force on the superhydrophobic coatings. As shown in Fig. 5b_1 to b_2, water droplets were observed to slide off, sweeping all the water droplets in the rolling path. Water droplets eventually disappeared from the superhydrophobic coatings in Fig. 5b_3, which refreshed the rolling path.

For another situation, water droplets could be stocked if smaller water droplets are on the rolling path. During the rolling process, as shown in Fig. 5c and Supporting Video S2, droplet 1 firstly merged with droplet 2 on the rolling path 1 (P1), followed by droplets 3 and 4. It is eventually stuck on the surface because of less volume input from droplets on its rolling path, see Fig. 5c_1 and c_2. The same phenomenon was observed in the sliding process of droplet 5 due to only several small size water droplets on the rolling path 2 (P2). Although both water droplets stuck on the coatings, the rolling paths were also free from water, see Fig. 5c_3. Consequently, the stuck water droplets were metastable, and sliding behavior may be triggered in another coalescence process. In contrast, the water accumulated on the bare surface was completely frozen into ice, resulting in the degradation of the surface.

To illustrate the sweeping behavior on superhydrophobic coatings, we developed a numerical model of the coalescence and sweeping process. As illustrated in Fig. 5d,

the direct condensation process is achieved by the low surface adhesion of the superhydrophobic coatings. During the condensation, droplet A presents higher adhesion strength due to its larger liquid-solid contact area. The distance (D_x) between droplet A and the adjacent droplet x is the critical data for coalescence. If the D_x is smaller than the sum of the radius of droplet A (r_A) and adjacent droplets x (r_x) $D_X < r_A + r_x$, the adjacent droplets are inevitably merged. The vicinity of droplet A is refreshed while its volume keeps growing, leading to the increment of droplet size ($r_{A`}$ or $r_{A``}$). When the size of coalesced droplet reaches its critical size, its adhesion strength cannot withstand gravity [38]. At this time, the rolling will be triggered, causing droplet A`` slides down the coatings, which sweep off all the water droplets on the rolling path, resulting in an increased droplet size (r_{A1} or r_{A2}), as shown in Fig. 5e. The coalescence provides more energy for sliding against the adhesion. However, the smaller droplets may not provide enough energy for sliding but sticking on the coatings. Therefore, the as-prepared coatings displayed good anti-icing properties even for the freezing rain at a micrometer scale.

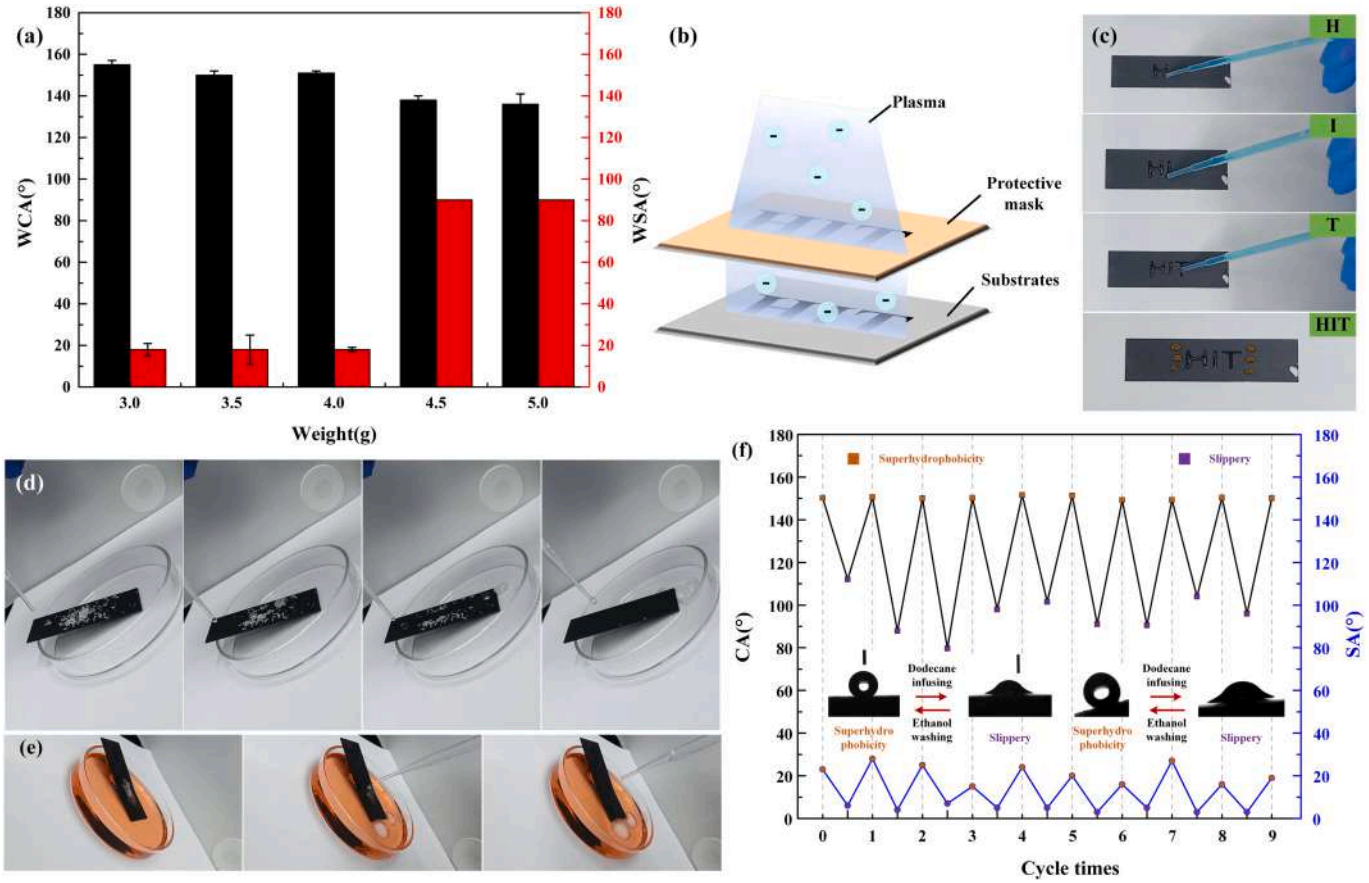

Fig. 4. (a) Wettability of as-prepared coatings in Effects of different mass ratios of EP. (b) Schematic of the information transfer process when irradiated by oxygen atmosphere plasma and (c) the developing process when wetted by water. (d) and (e) the self-cleaning performance of the as-prepared coatings at air condition and dodecane immersion, respectively. (f) The reversible wettability of superhydrophobic coatings EP-4 and slippery coatings at different cycles.

De-icing from a surface refers to the capability of removing ice. A snowy day was chosen to investigate the de-icing performance of the as-prepared superhydrophobic coatings, where the temperature was −10 °C at Harbin, China. From Fig. 6a, snow on the superhydrophobic coating EP-4 was quickly melted after being illuminated by IR light (808 nm, 1 W) for 45 s. The melted water accumulated to form water droplets after 76 s due to the low adhesion force of the coatings. After being illuminated for 165 s, almost half of the surface was free from snow, and new water balls appeared. However, the snow on the bare surface cannot be melted, although it was illuminated for another 45 s ($t = 210$ s). The coated and bare samples were completely covered with snow after being left outdoors overnight. The samples were exposed to sunlight the next day at an outdoor temperature of −10 °C. As shown in Fig. 6b, over 90 % of the coated surface was free from snow which is larger than the bare sample (about 60 %). In the meantime, it was found that the adjacent region outside the coated sample is also free from snow, with a width (~d) of about ~2 cm, possibly due to the heat dispersion from photothermal effects. The unique de-icing performance indicates the presence of photothermal effects on the superhydrophobic coatings. From the thermograph in Fig. 6c, it showed that the average temperature of snow was approximately 0 °C under the direct illumination of sunlight. And the melting process was significantly accelerated on superhydrophobic coatings, where the average surface temperature was around 12 °C, much higher than the ice melting point. In contrast, the average surface temperature of the bare sample was lower than 0 °C and the coldest region was about −10.4 °C. Consequently, the melting process was slowed down on bare samples, leading to larger snow-covered regions. Therefore, the as-prepared superhydrophobic coatings can improve the de-icing property due to its effective photothermal performance.

Furthermore, we investigated the ice removal property of as-prepared coatings once a mass of snow accumulation occurred. When a bulk of snow was deliberately placed on both surfaces with a tilt angle of 30°, it was observed that the snow on superhydrophobic coatings began to melt and slid off after 902 s and completely disappeared after 1242 s. However, the sliding speed of snow on the bare surface was slower without obvious melting. Therefore, the photothermal effect of the superhydrophobic surface EP-4 contributes to the melting and sliding of snow/ice. As illustrated in Fig. 6e, the melted snow at the interface forms a thin water film, acting as a slippery film. As a result, the accumulated snow/ice could be repelled and removed easily due to the Cassie state with the presence of surface air pockets, which dramatically increases the de-icing efficiency.

3.4. *Improved anti-/de-icing performance on as-prepared slippery surfaces*

As discussed in Sections 3.1 and 3.2, the hierarchical structures of as-prepared superhydrophobic coatings provide a high capacity for air and dodecane. The newly developed slippery surface could expand the potential applications of superhydrophobic coatings. For anti-icing application, the water dynamics on the as-prepared samples were investigated by a high-speed camera at room temperature. For comparison, a single water droplet was released from a height of 10 cm and reached the impact velocity (V_0) of 1.4 m/s before hitting on the samples, including the bare aluminum alloy, superhydrophobic surface EP-4, and improved slippery surface. Here, the non-dimensional parameter α (D/D_0, where D is the diameter of the water droplet and D_0 is the side

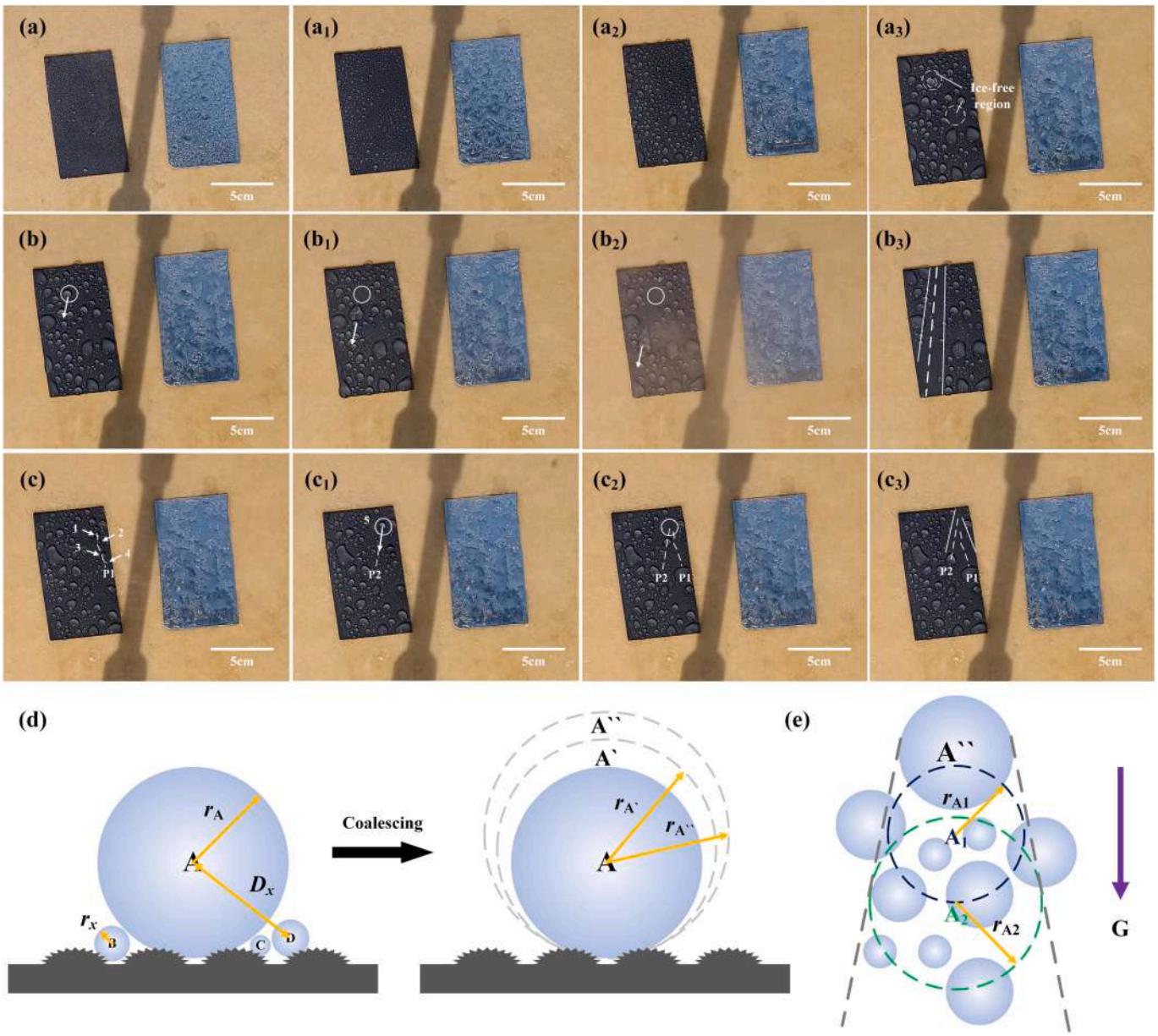

Fig. 5. (a)-(a_3) Images of water accumulation on as-prepares superhydrophobic surface and bare tinplate surface after spraying with supercold water 11, 21, 49, and 79 times. (b)-(b_1) Images of the water sliding process after spraying for 80 and (b_2)- (b_3) 81 times. (c)- (c_3) Images of the water sliding process after spraying 149 times. (d) Schematic of coalescence process on superhydrophobic coatings and (e) the water-sweeping process.

length of the samples) is defined to characterize the dynamic diameter ($D_{dynamic}$) of impacting water droplet. The impacting process of water droplets on tested samples were recorded in Supporting Videos S3 to S5.

As shown in Figs. 7a and S3, water droplets spread to the maximum diameter (D_{max}) on the bare surface within ($t_{b,spreading}$) ~15.6 ms and kept at a static state after ($t_{b,retraction}$) ~46.7 ms. The water droplet finally adhered to the bare surface, and the static diameter (D_{static}) was twice lower than D_{max}. As shown in Figs. 7b and S4, however, the dynamic behavior of water droplets on the superhydrophobic surface differed from that on the bare surface, which experienced three times of spreading, retraction, and rebounding cycles before rolling off the surface. At the first cycle, the water droplet reached D_{max} within ($t_{shs,spreading}$) ~4.4 ms, over three times shorter than the bare surface. Its retraction process was also three times faster with a reduced retraction time of ($t_{shs,retraction}$) ~14.4 ms. It spent ($t_{shs,rebounding}$) ~53.3 ms at the first rebounding process. Afterward, the impacting energy was rapidly dissipated in the following two cycles. For the second cycle, the D_{max} was reduced to four times smaller than the first cycle, but the spreading process was achieved within 5.6 ms, which was as fast as that in the first cycle. Comparing the rebounding time at the three cycles, the time interval of cycles 2 and 3 were 35.6 ms and 20 ms, respectively. It showed that the rebounding time became shorter, indicating the energy loss at each impacting process. Eventually, the water droplets jumped and rolled off the superhydrophobic surface EP-4.

As to the slippery surface, the water droplet showed a similar spreading and retraction process to the bare surface, although it kept sliding on the slippery surface at the final stage. During the impacting process, it took ($t_{s,spreading}$) ~12.2 ms before the water droplet reached the D_{max} and ($t_{s,retraction}$) ~27.8 ms at the retraction process, see Figs. 7c and Fig. S5. It showed shorter spreading and retraction times than those on the bare surface. The maximum diameter of water droplets on the slippery surface was presented to be the largest, following α_{bare} (0.44) < $\alpha_{superhydrophobic}$ (0.51) < $\alpha_{slippery}$ (0.69). Afterward, the water droplets kept sliding on the slippery surface, leading to the diameter fluctuation

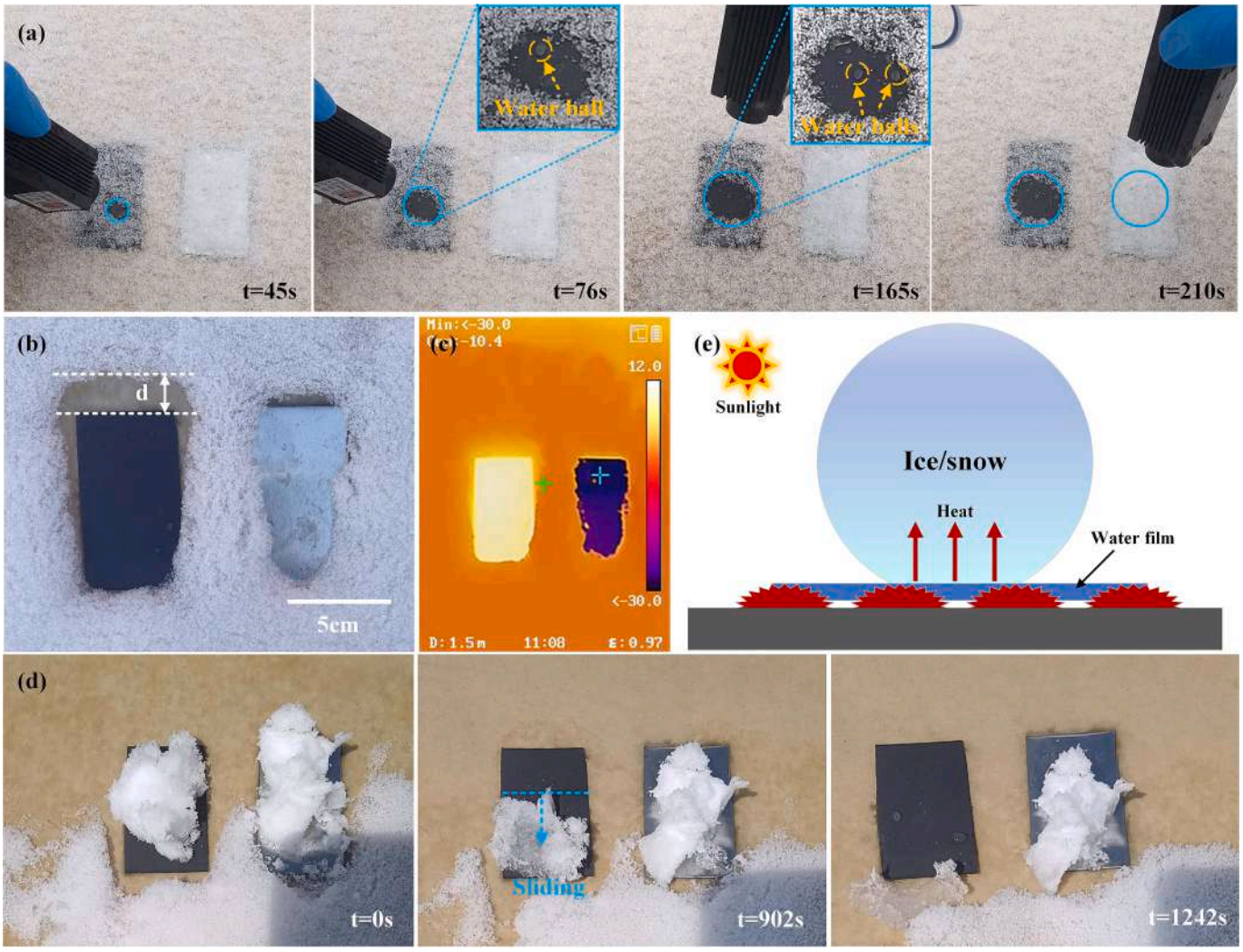

Fig. 6. (a) Investigation of snow melting behavior on the superhydrophobic coatings EP-4 and bare tinplate surface after being illuminated by IR light (808 nm, 1 W). (b) Investigation of snow melting behavior after exposure to sunlight over 3 h, and (c) the thermograph captured by a hand-held thermal imager. (d) Investigation of de-icing behavior of tested samples covered by a bulk of snow. (e) Schematic of ice/snow sliding behavior under photothermal effect on superhydrophobic coatings EP-4.

before the final stop.

The impacting models of water dynamics on the three representative surfaces were illustrated in Figs. 7d-f. For the bare aluminum alloy surface (see Fig. 7d), the water droplet completely contacts the solid surface, resulting in the energy loss during the spreading and retraction process. Consequently, water droplet was stuck at the contacting site due to the high adhesion force of the metal surface. The water droplet impacting model for the superhydrophobic surface is proposed in Fig. 7e. The air pockets can be compressed by the high-speed water droplet during the impacting process, which provides the supporting force for the water droplet to rebounding from the surface [39]. In addition, the low surface energy helps to reduce the energy loss during the spreading and retraction process. Therefore, the impact process of water droplets on the superhydrophobic surface presented a fast and repeated bouncing behavior due to the preserved kinetic energy during the impacting process. In comparison, the lubricant (dodecane), filling in the micro-gaps plays the similar role like the air pockets, see Fig. 7f. The water droplet is completely repelled during the impacting process on the slippery surface because of the sliding at the liquid-liquid contact [40]. The low surface friction of the lubricant enables the water droplet to slide along the slippery surface due to less energy loss than on the bare surface. Therefore, both the superhydrophobic and slippery surfaces exhibit potential icephobic properties in a cold environment, which makes it possible to improve the icephobic performance by shifting the surface wettability smartly.

We further investigated the anti-icing property of the samples by evaluating their freezing delay performance. A homemade apparatus was employed to record the frozen process of water droplets in a sealed chamber, as shown in Fig. S1. To quantitatively characterized the frozen process, its inner temperature was precisely controlled by two electronic temperature controllers, and the minimum temperature could reach −40 °C. The bare aluminum alloy surface, superhydrophobic coatings, and slippery coatings were placed on a platform in the cold chamber. When the temperature of the hermetic space was decreased to 0 °C, a water droplet (50 μL) was placed on all tested sample surfaces simultaneously and frozen at the cooling rate of 0.43 °C/min.

As shown in Fig. 8a-c, it is observed that the bottom part of the water droplet on all tested samples was solidified first, but its top part remained as liquid (or supercooled state). From Fig. 8a, it took 2196 s before the water droplets became opaque on the bare sample surface, which was recognized as the onset of icing process. And the freezing line for the water droplet gradually went up on the bare surface as the freezing proceeded. Eventually, the water droplets on bare surface completely froze after 2239 s and changed to a “semi-peach” shape.

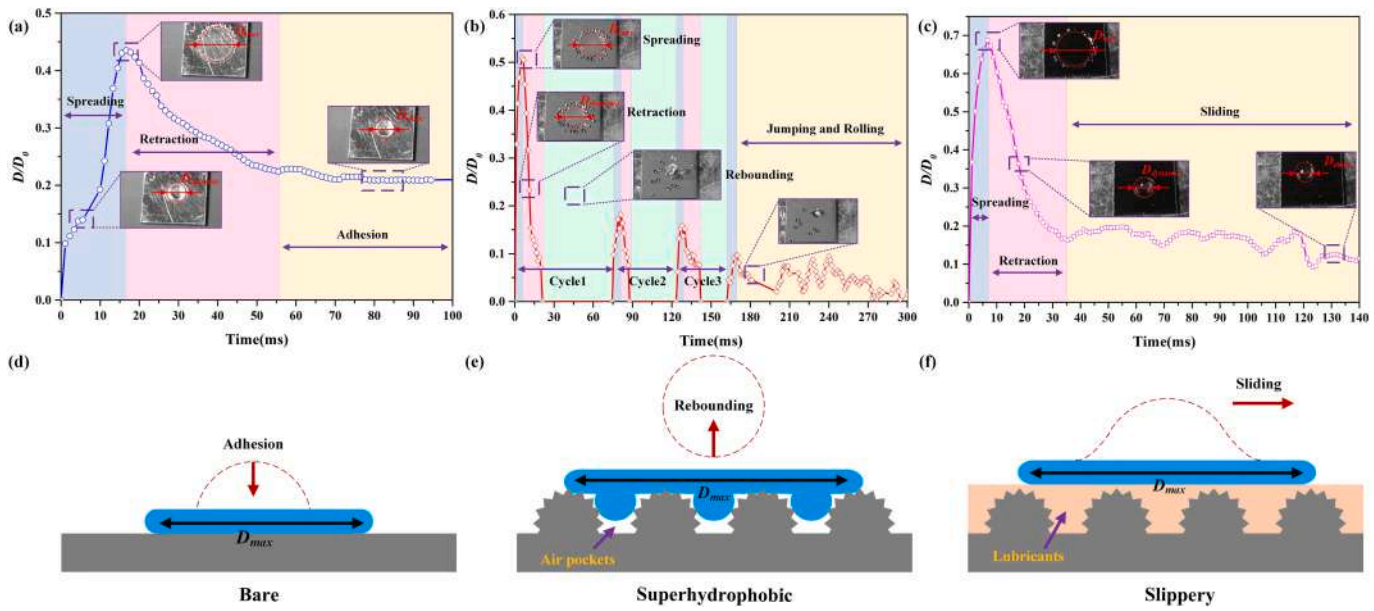

Fig. 7. Dynamic process of a single water droplet on (a) bare aluminum alloy surface, (b) superhydrophobic surface EP-4, (c) the slippery surface. Insets are the impacting images of water droplets captured by a high-speed camera. (d-f) The corresponding impacting mechanism of water droplets to (a-c).

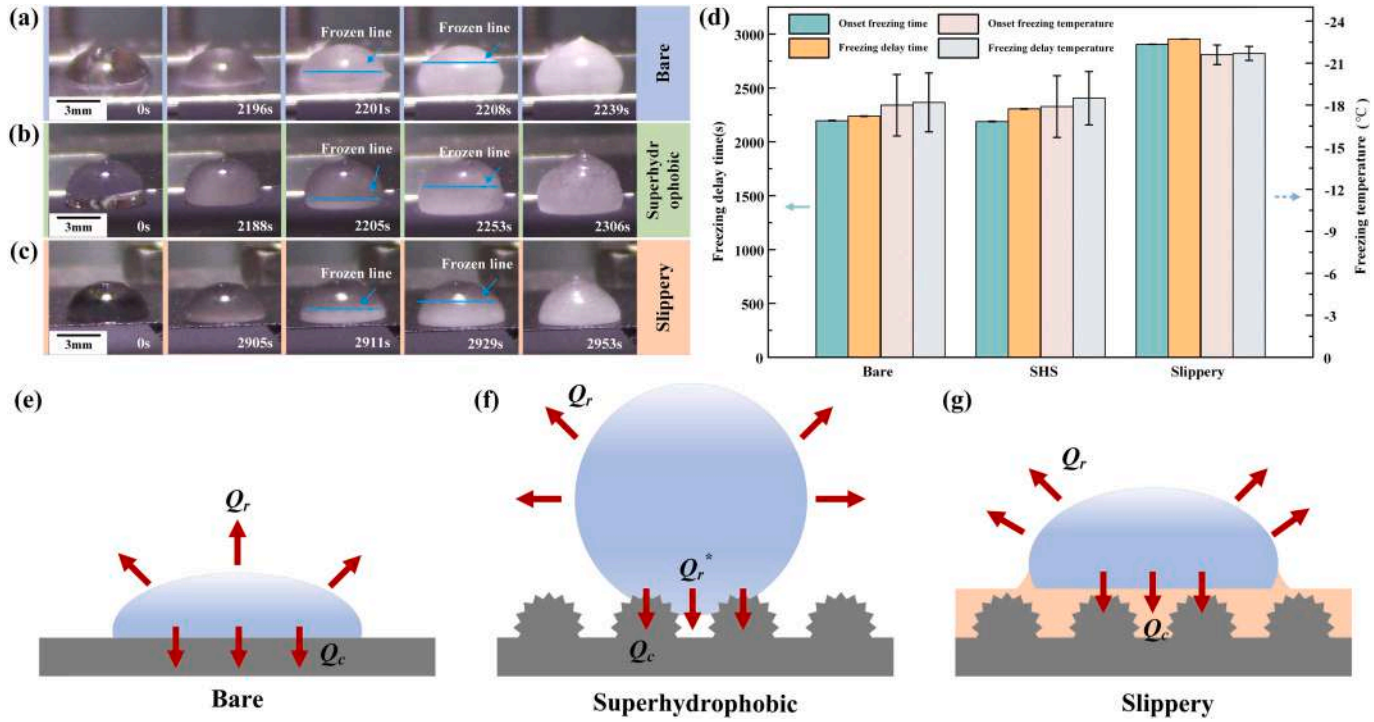

Fig. 8. (a)-(c) Images of the icing process of water droplets on bare aluminum alloy surface, superhydrophobic coatings EP-4, and as-prepared slippery coatings, respectively. (d) Freezing delay time and the corresponding freezing temperatures on the tested samples. (e)-(g) Schematics of heat transfer process on the tested samples.

From Fig. 8b and c, the onset of freezing time (t_o) on the superhydrophobic and slippery coatings were 2188 and 2905 s, respectively. Comparing to the bare surface, the rising speed of freezing line was dramatically lowered, which took 118 s before the droplets were frozen into a "peach" shape. On the contrary, the rising speed of freezing line on the bare surface and slippery surface were faster, which were 43 and 48 s, respectively. And the freezing delay time (t_d) on slippery coatings was the longest (~2953 s), indicating the improved anti-icing performance on slippery coatings. Correspondingly, the temperature when freezing started (T_f) on bare surfaces was −18 °C, and the temperature when icing completed (T_i) was −18.2 °C, as shown in Fig. 8d. And the T_f and T_i on the superhydrophobic surfaces were − 17.9 °C and − 18.5 °C, respectively. The temperature difference on superhydrophobic surface was dramatic (0.6 °C), showing that the heat loss at frozen process was greatly depressed. Meanwhile, the T_f and T_i on slippery surfaces were further decreased to −21.6 and − 21.7 °C, respectively. Therefore, freezing delay performance of superhydrophobic coatings can be improved by actively altering its wettability.

Here, the heat transfer models were established to demonstrate the mechanisms of different icing process on the representative surfaces. Generally, there was no energy input path for the water droplets but only by heat loss due to the cold hermetic environment. As illustrated in Fig. 8e, the heat loss of water droplets on the bare surface (ΔQ_{lW}) includes two main terms because of the Wenzel state, i.e., by conduction, Q_{cw}, or by natural convection, Q_{rw}. The total heat loss is expressed as [41]:

$$\Delta Q_{lW} = Q_{cw} + Q_{rw} \quad (1)$$

However, water droplets in Cassie state are suspended over the hierarchical structures due to air pockets. As shown in Fig. 8f, heat radiation through the air cushion (Q^*_{rc}) should be involved during the heat loss process. The total heat loss, ΔQ_{lC}, can be written as [41–43]:

$$\Delta Q_{lC} = Q_{cc} + Q_{rc} + Q^*_{rc} \quad (2)$$

As for the slippery coatings, the terms for the heat transfer should include the lubricant, the hierarchical structures, and the surface coating thickness [44]. Since the water droplets generally nucleated within the lubricant layer [45], the heat transfer on a slippery surface (ΔQ_{lS}) can be simplified, mainly including the conduction heat loss through the lubricant layer and the convection heat loss, as shown in Fig. 8g. The heat loss mechanism is similar to the Wenzel state, described as:

$$\Delta Q_{lS} = Q_{cs} + Q_{rs} \quad (3)$$

However, dodecane as the lubricant is often a good candidate for phase change material (PCM) with a phase change at −9.6 °C [46]. The deposited dodecane replaces the air pockets, supported by the skeleton of the hierarchical structure. Consequently, the dodecane in the liquid phase releases the latent heat when its temperature decreases to its phase-transition temperature [47]. The released latent heat can be transferred to the water droplets, delaying ice formation. To include the latent heat of dodecane, Q_{lh}, the heat loss on the slippery surface (ΔQ_{lS}) can be updated as:

$$\Delta Q_{lS} = Q_{cs} + Q_{rs} - Q_{lh} \quad (4)$$

Considering the freezing delay time (t) on the tested samples was $t_s > t_c > t_w$, the total heat loss rates (η) of the tested samples follow $\eta_w > \eta_c > \eta_s$. It can be concluded that the existence of air pockets and lubricants within the hierarchical structures at the interface can dramatically reduce the heat loss to the substrates. Therefore, the superhydrophobic coating not only displays good anti-icing performance, but also it can be developed to a slippery surface with improved functionality by employing the PCM as the lubricants.

In addition to the delayed freezing performance, the ice-removal performance was also evaluated by measuring the ice shearing strength (ISS). The tested samples were first fixed on the platform, on which the water column was frozen into the tested ice cube after 15 min, as shown in Fig. 9a and Fig. S1. The ISS was measured by a force sensor. Fig. 9b shows that the ISS of the EP-3 and EP-3.5 coatings were 175.8 ± 3.8 and 193.6 ± 7.6 kPa, respectively, higher than that of the bare aluminum alloy surface (163 ± 5.1 kPa). The increase of ISS should be attributed to the surface defects of the as-prepared coatings. And the unsatisfied superhydrophobic property dramatically influenced the ISSs of the EP-4.5 and EP-5, i.e. 175.8 ± 2.5 and 178.3 ± 10.2 kPa, respectively. The EP-4 sample showed better ice removal performance with the lowest ISS of 129.9 ± 12.7 kPa. After being infused with dodecane, the ISS of the slippery coating was two times lower than bare surfaces, which is 77.7 ± 6.4 kPa. The difference in the ice removal performance should be attributed to the interfacial interaction between the ice and the substrates, as shown in Fig. 9c. For bare surface, the iced area (S_{iw}) could be larger than the projected area of ice column (S_{proj}), $S_{iw} > S_{proj}$. However, the three-phase contact line on superhydrophobic coating is intermittent. The iced area (S_{ic}) is smaller than the S_{proj}, $S_{ic} < S_{proj}$, resulting in a lower ISS than that of the bare surface ($F_c = \tau_c \cdot S_{ic} < F_w = \tau_w \cdot S_{iw}$). For the slippery coating, the ice column is completely in contact with the lubricant film. The iced area of ice column on the slippery coating (S_{is}) can be regarded as equal to the S_{proj}. In contrast to the direct contact with the substrates, the adhesion strength between ice and lubricant (τ_s) is much lower than that on the bare surface (τ_w) and the superhydrophobic coating (τ_s). Therefore, the ISS of as-prepared slippery coating was the smallest ($F_s = \tau_s \cdot S_{is} < F_c < F_w$), where ice has a high tendency of slippage [48]. Therefore, the de-icing performance of a superhydrophobic coating can be improved if replacing the air pockets with lubricants. In addition, the ice shear strength of slippery sample was further evaluated to characterize its icing removal durability. As shown in Fig. S6, the ice shear strength of the as-prepared slippery sample gradually increased. After 6 icing cycles, the ISS (~148 kPa) was still lower than that of the bare surface. The results should be attributed to the exposure of micro-nanostructures by peeling the lubrication layer during repeated shearing process, leading to the degradation of ice removal performance.

4. Conclusion

In summary, a series of superhydrophobic coatings with hierarchical structures at micro/nano-scale are fabricated using a simple spraying method on different substrates. The superhydrophobic surface EP-4 presents a high θ_{CA} of ~151 ± 1° and a low θ_{SA} of ~18 ± 3°. After being infused with dodecane, the as-prepared surface displays ultra-slippery properties, where the θ_{CA} and θ_{SA} are ~112° and ~ 6°, respectively. Moreover, the wettability of the as-prepared coatings can smartly reverse between the superhydrophobic and the slippery surfaces

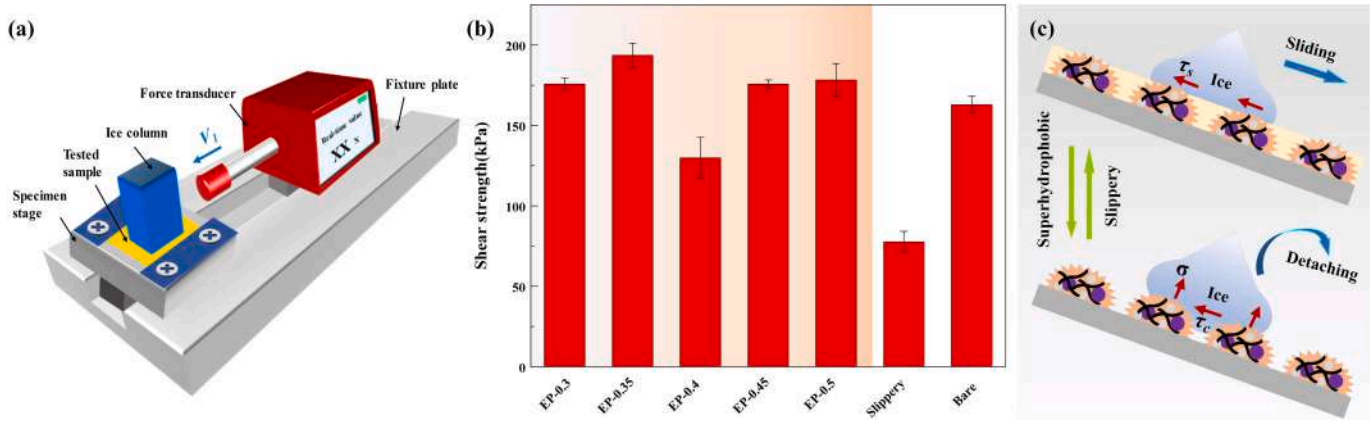

Fig. 9. Schematic diagram of the ice adhesion evaluation of an in-house equipment. (b) Ice shear strength of different tested samples. (c) Schematic of the detaching mechanism of ice column on bare aluminum alloy surface, superhydrophobic coatings EP-4, and as-prepared slippery coatings, respectively.

on demand with good reversibility after 9 washing and infusing cycles, exhibiting a bi-stable state. For the superhydrophobic samples, the outdoor freezing-rain tests show that the supercold water droplets can aggregate to form oversized droplets larger than the critical diameters, which can roll off by gravity at −14 °C. The accreted snow covering over 90 % of the coated area was quickly melted within 165 s at −10 °C after being illuminated with IR light (808 nm, 1 W) due to the photothermal effects. The superhydrophobic samples also presents good water-repellent properties, on which water droplets quickly roll off with a fast spreading and retraction performance. For the slippery state, the impacting water droplets quickly reaches the D_{max} within ($t_{s,\ spreading}$) ~12.2 ms and slide along the surface due to the low surface friction. Meanwhile, the freezing delaying time on the slippery coating is 2953 s, better than that on the superhydrophobic surface. The ISS of the slippery surface is 77.7 ± 6.4 kPa, two times lower than the bare surfaces. The results show that the reversible superhydrophobic and slippery coatings can offer excellent anti-icing and de-icing performance, expanding the service conditions of certain functional coatings. Therefore, we believe this study will provide insights for developing multifunctional coatings in adaption to different service environments for future anti-icing and de-icing applications.

Supplementary data to this article can be found online at https://doi.org/10.1016/j.porgcoat.2023.107754.

CRediT authorship contribution statement

Xinlin Li (First Author): Conceptualization, Methodology, Investigation, Visualization, Writing - Original Draft;

Zhe Zhao: Investigation, Visualization;

Yan Liu (Corresponding Author): Conceptualization, Resources;

Yanju Liu (Corresponding Author): Conceptualization, Validation, Review & Editing;

Jinsong Leng (Corresponding Author): Resources, Supervision, Review & Editing.

Declaration of competing interest

The authors declare that there is no actual or potential conflict of interest in relation to this article.

Data availability

Data will be made available on request.

Acknowledgements

This work was supported by the following funds: National Natural Science Foundation of China (No. 12102105), China Postdoctoral Science Foundation (No. 2021M690834), and Postdoctoral Science Foundation of Heilongjiang Province (No. LBH-Z21156), and Opening Project of the Key Laboratory of Bionic Engineering (Ministry of Education), Jilin University (No. KF20211003).

References

[1] T.C. Maloney, F.J. Diez, T. Rossmann, Ice accretion measurements of jet a-1 in aircraft fuel lines, Fuel 254 (2019), 115616.
[2] S. Mintu, D. Molyneux, Ice accretion for ships and offshore structures. Part 1-state of the art review, Ocean Eng. 258 (2022), 111501.
[3] X. Huang, N. Tepylo, V. Pommier-Budinger, M. Budinger, E. Bonaccurso, P. Villedieu, L. Bennani, A survey of icephobic coatings and their potential use in a hybrid coating/active ice protection system for aerospace applications, Prog. Aeosp. Sci. 105 (2019) 74–97.
[4] Y. Shen, X. Wu, J. Tao, C. Zhu, Y. Lai, Z. Chen, Icephobic materials: fundamentals, performance evaluation, and applications, Prog. Mater. Sci. 103 (2019) 509–557.
[5] Z. Wang, B. Lin, S. Sheng, S. Tan, P. Wang, Y. Tao, Z. Liu, Z. He, J. Wang, Bioinspired anti-icing hydrogel enabled by ice-nucleating protein, Ccs Chem. 4 (1) (2022) 104–111.
[6] G. Bai, D. Gao, Z. Liu, X. Zhou, J. Wang, Probing the critical nucleus size for ice formation with graphene oxide nanosheets, Nature 576 (7787) (2019) 437–441.
[7] K. Liu, C. Wang, J. Ma, G. Shi, X. Yao, H. Fang, Y. Song, J. Wang, Janus effect of antifreeze proteins on ice nucleation, Proc. Natl. Acad. Sci. 113 (51) (2016) 14739–14744.
[8] V. Rico, J. Mora, P. García, A. Agüero, A. Borrás, A.R. González-Elipe, C. López-Santos, Robust anti-icing superhydrophobic aluminum alloy surfaces by grafting fluorocarbon molecular chains, Appl. Mater. Today 21 (2020), 100815.
[9] H. Wang, G. Chi, Y. Wang, F. Yu, Z. Wang, Fabrication of superhydrophobic metallic surface on the electrical discharge machining basement, Appl. Surf. Sci. 478 (2019) 110–118.
[10] F. Mayoussi, E.H. Doeven, A. Kick, A. Goralczyk, Y. Thomann, P. Risch, R.M. Guijt, F. Kotz, D. Helmer, B.E. Rapp, Facile fabrication of micro−/nanostructured, superhydrophobic membranes with adjustable porosity by 3d printing, J. Mater. Chem. A 9 (37) (2021) 21379–21386.
[11] C. Yan, P. Jiang, X. Jia, X. Wang, 3d printing of bioinspired textured surfaces with superamphiphobicity, Nanoscale 12 (5) (2020) 2924–2938, https://doi.org/10.1039/c9nr09620e.
[12] D. Wei, J. Wang, Y. Liu, D. Wang, S. Li, H. Wang, Controllable superhydrophobic surfaces with tunable adhesion on mg alloys by a simple etching method and its corrosion inhibition performance, Chem. Eng. J. 404 (2021), 126444.
[13] I.S. Bayer, Superhydrophobic coatings from ecofriendly materials and processes: a review, Adv. Mater. Interfaces 7 (13) (2020) 2000095.
[14] D. Li, L. Ma, B. Zhang, S. Chen, Large-scale fabrication of a durable and self-healing super-hydrophobic coating with high thermal stability and long-term corrosion resistance, Nanoscale 13 (16) (2021) 7810–7821, https://doi.org/10.1039/d0nr08985k.
[15] N. Celik, I. Torun, M. Ruzi, A. Esidir, M.S. Onses, Fabrication of robust superhydrophobic surfaces by one-step spray coating: evaporation driven self-assembly of wax and nanoparticles into hierarchical structures, Chem. Eng. J. 396 (2020), 125230.
[16] M. Aliabadi, W. Konrad, T. Stegmaier, Y. Liu, B. Zhan, G. Wang, C. Kaya, G. Gresser, Modeling of self-driven directional movement of underwater oil droplets on bio-inspired nano-coated 3d-printed conical models, Sep. Purif. Technol. 305 (2023), 122405.
[17] M.J. Kreder, J. Alvarenga, P. Kim, J. Aizenberg, Design of anti-icing surfaces: smooth, textured or slippery? Nat. Rev. Mater. 1 (1) (2016) 1–15.
[18] L. Wang, J. Li, Z. Chen, Z. Song, X. Meng, X. Chen, Porous graphene-based photothermal superhydrophobic surface for robust anti-icing and efficient de-icing, Adv. Mater. Interfaces (2022) 2201758.
[19] Z. Zhao, H. Chen, Y. Zhu, X. Liu, Z. Wang, J. Chen, A robust superhydrophobic anti-icing/de-icing composite coating with electrothermal and auxiliary photothermal performances, Compos. Sci. Technol. 227 (2022), 109578.
[20] H. Chen, P. Zhang, L. Zhang, H. Liu, Y. Jiang, D. Zhang, Z. Han, L. Jiang, Continuous directional water transport on the peristome surface of nepenthes alata, Nature 532 (7597) (2016) 85–89.
[21] F. Wang, Y. Zhuo, Z. He, S. Xiao, J. He, Z. Zhang, Dynamic anti-icing surfaces (dais), Adv. Sci. 8 (21) (2021) 2101163.
[22] G. Wang, Z. Guo, Liquid infused surfaces with anti-icing properties, Nanoscale 11 (47) (2019) 22615–22635, https://doi.org/10.1039/c9nr06934h.
[23] R. Pan, H. Zhang, M. Zhong, Triple-scale superhydrophobic surface with excellent anti-icing and icephobic performance via ultrafast laser hybrid fabrication, ACS Appl. Mater. Interfaces 13 (1) (2020) 1743–1753.
[24] Y. Long, X. Yin, P. Mu, Q. Wang, J. Hu, J. Li, Slippery liquid-infused porous surface (slips) with superior liquid repellency, anti-corrosion, anti-icing and intensified durability for protecting substrates, Chem. Eng. J. 401 (2020), 126137.
[25] M. Carlotti, I. Cesini, V. Mattoli, A simple approach for flexible and stretchable anti-icing lubricant-infused tape, ACS Appl. Mater. Interfaces 13 (37) (2021) 45105–45115.
[26] R. Chatterjee, U. Chaudhari, S. Anand, How to select phase change materials for tuning condensation and frosting? Adv. Funct. Mater. 2206301 (2022).
[27] M. Shamshiri, R. Jafari, G. Momen, An intelligent icephobic coating based on encapsulated phase change materials (pcm), Colloids Surf. A Physicochem. Eng. Asp. 655 (2022), 130157.
[28] R. Chatterjee, D. Beysens, S. Anand, Delaying ice and frost formation using phase-switching liquids, Adv. Mater. 31 (17) (2019) 1807812.
[29] S. Zhang, D. Feng, L. Shi, L. Wang, Y. Jin, L. Tian, Z. Li, G. Wang, L. Zhao, Y. Yan, A review of phase change heat transfer in shape-stabilized phase change materials (ss-pcms) based on porous supports for thermal energy storage, Renew. Sust. Energ. Rev. 135 (2021), 110127.
[30] F. Wang, W. Ding, J. He, Z. Zhang, Phase transition enabled durable anti-icing surfaces and its diy design, Chem. Eng. J. 360 (2019) 243–249.
[31] I. Hejazi, G.M.M. Sadeghi, J. Seyfi, S. Jafari, H.A. Khonakdar, Self-cleaning behavior in polyurethane/silica coatings via formation of a hierarchical packed morphology of nanoparticles, Appl. Surf. Sci. 368 (2016) 216–223.
[33] M. Aghvami-Panah, A. Wang, M. Panahi-Sarmad, S.A.S. Esfahani, A.A. Seraji, M. Shahbazi, R. Ghaffarian, S. Jamalpour, X. Xiao, A comparison study on polymeric nanocomposite foams with various carbon nanoparticles: adjusting radiation time and effect on electrical behavior and microcellular structure, Int. J. Smart Nano Mater. 13 (3) (2022) 504–528.
[34] P. Chauhan, A. Kumar, B. Bhushan, Self-cleaning, stain-resistant and anti-bacterial superhydrophobic cotton fabric prepared by simple immersion technique, J. Colloid Interface Sci. 535 (2019) 66–74.
[35] J. Ou, F. Wang, W. Li, M. Yan, A. Amirfazli, Methyltrimethoxysilane as a multipurpose chemical for durable superhydrophobic cotton fabric, Prog. Org. Coat. 146 (2020), 105700.

[36] F. Wang, R. Ma, J. Zhan, W. Shi, Y. Zhu, Y. Tian, Superhydrophobic/superoleophilic starch-based cryogels coated by silylated porous starch/fe3o4 hybrid micro/nanoparticles for removing discrete oil patches from water, Sep. Purif. Technol. 291 (2022), 120872.
[37] S. Xu, Q. Wang, N. Wang, Chemical fabrication strategies for achieving bioinspired superhydrophobic surfaces with micro and nanostructures: a review, Adv. Eng. Mater. 23 (3) (2021) 2001083.
[38] P.B. Weisensee, Y. Wang, H. Qian, D. Schultz, W.P. King, N. Miljkovic, Condensate droplet size distribution on lubricant-infused surfaces, Int. J. Heat Mass Transf. 109 (2017) 187–199.
[39] H. Lambley, T.M. Schutzius, D. Poulikakos, Superhydrophobic surfaces for extreme environmental conditions, Proc. Natl. Acad. Sci. 117 (44) (2020) 27188–27194.
[40] H. Luo, S. Yin, S. Huang, F. Chen, Q. Tang, X. Li, Fabrication of slippery zn surface with improved water-impellent, condensation and anti-icing properties, Appl. Surf. Sci. 470 (2019) 1139–1147.
[41] X. Li, G. Wang, A.S. Moita, C. Zhang, S. Wang, Y. Liu, Fabrication of bio-inspired non-fluorinated superhydrophobic surfaces with anti-icing property and its wettability transformation analysis, Appl. Surf. Sci. 505 (2020), https://doi.org/10.1016/j.apsusc.2019.144386.
[42] A. Criscione, I.V. Roisman, S. Jakirlić, C. Tropea, Towards modelling of initial and final stages of supercooled water solidification, Int. J. Therm. Sci. (2015), https://doi.org/10.1016/j.ijthermalsci.2015.01.021.
[43] M. Schremb, S. Borchert, E. Berberovic, S. Jakirlic, I.V. Roisman, C. Tropea, Computational modelling of flow and conjugate heat transfer of a drop impacting onto a cold wall, Int. J. Heat Mass Transf. (2017), https://doi.org/10.1016/j.ijheatmasstransfer.2017.02.073.
[44] J. Zhang, W. Zhang, J. Lu, C. Zhu, W. Lin, J. Feng, Aqueous epoxy-based superhydrophobic coatings: fabrication and stability in water, Prog. Org. Coat. 121 (2018) 201–208.
[45] T. Kajiya, F. Schellenberger, P. Papadopoulos, D. Vollmer, H. Butt, 3d imaging of water-drop condensation on hydrophobic and hydrophilic lubricant-impregnated surfaces, Sci. Rep. (2016), https://doi.org/10.1038/srep23687.
[46] Y. Song, N. Zhang, Y. Jing, X. Cao, Y. Yuan, F. Haghighat, Experimental and numerical investigation on dodecane/expanded graphite shape-stabilized phase change material for cold energy storage, Energy 189 (2019), 116175.
[47] L. Song, C. Yang, S. Zhang, Y. Wang, R. Zou, E. Cheng, A. Lee, Q. Deng, Multifunctional photothermal phase-change superhydrophobic film with excellent light–thermal conversion and thermal-energy storage capability for anti-icing/de-icing applications, Langmuir 38 (49) (2022) 15245–15252.
[48] S. Barthwal, B. Lee, S. Lim, Fabrication of robust and durable slippery anti-icing coating on textured superhydrophobic aluminum surfaces with infused silicone oil, Appl. Surf. Sci. 496 (2019), 143677.